Journal of Applied Polymer Science

Electrochemical Synthesis and *In Situ* Spectroelectrochemistry of Conducting NMPy-TiO_2 and ZnO Polymer Nanocomposites for Li Secondary Battery Applications

Jalal Arjomandi,[1] Niloofar Keramat Irad Mossa,[1] Babak Jaleh[2]

[1]Department of Physical Chemistry, Faculty of Chemistry, Bu-Ali Sina University, 65178 Hamedan, Iran

[2]Physics Department, Bu-Ali Sina University, Hamedan, Iran

Dedicated to Professor Rudolf Holze on the occasion of his 60th birthday.

Correspondence to: J. Arjomandi (E-mail: j_arjomandi@basu.ac.ir)

ABSTRACT: Poly(*N*-methylpyrrole) (PNMPy), poly(*N*-methylpyrrole-TiO_2) (PNMPy-TiO_2), and poly (*N*-methylpyrrole-ZnO) (PNMPy-ZnO) nanocomposites were synthesized by *in situ* electropolymerization for cathode active material of lithium secondary batteries. The charge–discharging behavior of a Li/$LiClO_4$/PNMPy battery was studied and compared with Li/$LiClO_4$/PNMPy-nanocomposite batteries. The nanocomposites and PNMPy films were characterized by cyclic voltammetry, *in situ* resistivity measurements, *in situ* UV–visible, and Fourier transform infra-red (FTIR) spectroscopy, scanning electron microscopy (SEM), and transmission electron microscopy (TEM). The differences between redox couples (ΔE) were obtained for polymer nanocomposites and PNMPy films. During redox scan, a negative shift of potential was observed for polymer nanocomposite films. Significant differences from *in situ* resistivity of nanocomposites and PNMPy films were obtained. The *in situ* UV–visible spectra for PNMPy and polymer nanocomposite films show the intermediate spectroscopic behavior between polymer nanocomposites and PNMPy films. The FTIR peaks of polymer nanocomposite films were found to shift to higher wavelengths in PNMPy films. The SEM and TEM micrographs of nanocomposite films show the presence of nanoparticle in PNMPy backbone clearly. The result suggests that the inorganic semiconductor particles were incorporated in organic conducting PNMPy, which consequently modifies the properties and morphology of the film significantly. © 2014 Wiley Periodicals, Inc. J. Appl. Polym. Sci. **2015**, *132*, 41526.

KEYWORDS: applications; composites; conducting polymers; electrochemistry

Received 2 June 2014; accepted 14 September 2014

DOI: 10.1002/app.41526

INTRODUCTION

Conducting polymers such as polyaniline (PAn), polypyrrole (PPy), poly(*N*-methylpyrrole) (PNMPy), polythiophene (PTh), and their derivatives with different electrical or electrochemical properties have been studied extensively because of their many potential applications.[1–8] The electrochemical stability of poly-*N*-substituted pyrrole is better than that of the PPy.[9] However, the lower conductivity of their compounds makes them much less attractive than the parent molecule.[10–12] PPy and PNMPy aroused a great interest because of its large field of applications such as energy storage devices,[13,14] sensors and biosensors,[15,16] batteries,[17] solid-state devices,[18,19] conducting materials, corrosion inhibitors,[15] and others. In recent years, the developments of hybrid materials have been receiving significant attention due to wide ranges of potential applications in optoelectronic devices[16,17] and in field effect transistors.[20] The synthesis of polymer/inorganic nanocomposites materials has the goal of obtaining a new nanocomposite material having synergetic or complementary behaviors between the polymer and inorganic material.[21] Among the conducting polymers, PPy and PAn are the most studied polymers because of their relative ease in preparation and good environmental stability.[22,23] Between the inorganic materials, some metal oxides such as Fe_3O_4, MnO_2, TiO_2, NiO, and ZnO have been used for the synthesis of the nanocomposites with PAn or PPy.[21,24–27] Incorporation of nanostructures inorganic compounds into the conducting polymer will facilitate the combination of different features of organic and inorganic species. The inorganic fillers in the nano form are expected to modify the properties of the compound leading to the development of multifunctional devices.[28,29] The inorganic fillers at nanoscale exhibit high surface to volume ratio and thus expected to modify drastically the electrical, optical, and dielectric properties of polymers.[21] There are few reports on the synthesis, morphological, electrical, and optical studies of PAn

and PPy with TiO_2 and ZnO nanocomposites.[30–35] To the best of our knowledge, no attempt has been made to synthesis of PNMPy-TiO_2 and PNMPy-ZnO nanocomposites on gold electrode. However, electrodeposition of PNMPy in the presence of TiO_2 nanoparticles on steel was reported previously.[35] The electrochemical synthesis of PAn in the presence of TiO_2, ZnO, and TiO_2 + ZnO semiconductor on gold electrode has been reported as a first work on this area by us recently.[21] The results indicated the effect of nano-oxide materials on electropolymerization process and electrochemical activity. Here, we report the electrochemical synthesize of PNMPy in the presence of TiO_2 and ZnO as a hybrid materials by potential cycling on gold electrode. The resulting polymer films were characterized by *in situ* UV–visible, *ex situ* Fourier transform infra-red (FTIR) spectroscopy, scanning electron microscopy (SEM), transmission electron microscopy (TEM), and *in situ* conductivity measurements. The charge–discharging behavior of Li/$LiClO_4$/PNMPy and Li/$LiClO_4$/PNMPy-nanocomposite batteries were studied and compared too. The synthesis of PPy, PNMPy, PPy-*co*-PNMPy, or PNMPy with nano metal oxide films may expect

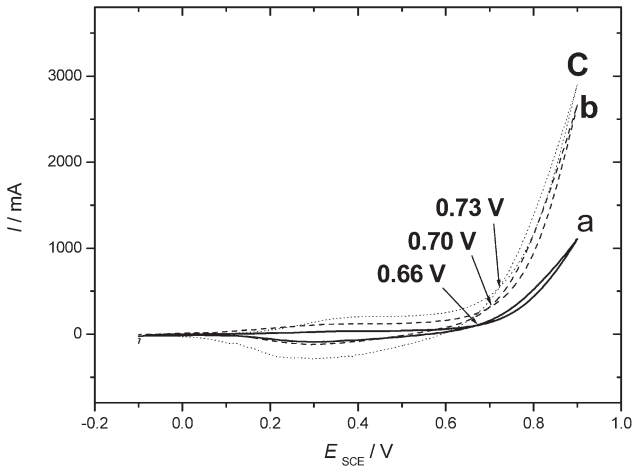

Figure 1. CVs of a gold electrode for (a) 0.1*M* NMPy (solid line), (b) 0.1*M* NMPy-TiO_2 (dashed line), and (c) 0.1 NMPy-ZnO (dotted line) in ACN +0.1*M* $LiClO_4$ nonaqueous solution in the potential range of −0.10 $< E_{SCE} <$ 0.90 V at $dE/dt = 50$ mV s^{-1}, respectively.

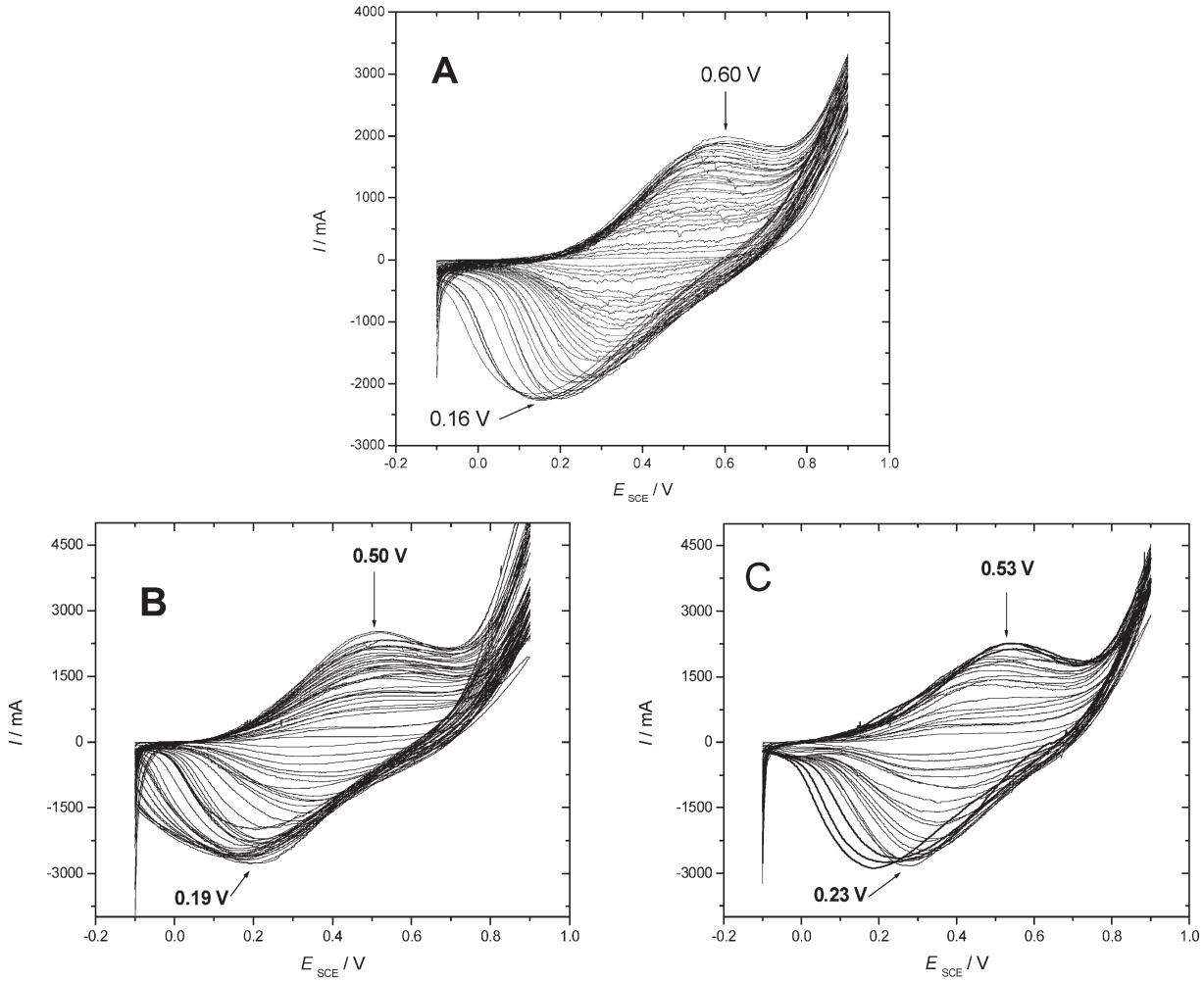

Figure 2. CVs (1, 2, 3,..., 40th cycles) during formation of (A) PNMPy, (B) PNMPy-TiO_2, and (C) PNMPy-ZnO nanocomposite polymer films in ACN +0.1*M* $LiClO_4$ nonaqueous solution in the potential range of −0.10 $< E_{SCE} <$ 0.90 V at $dE/dt = 50$ mV s^{-1}, respectively.

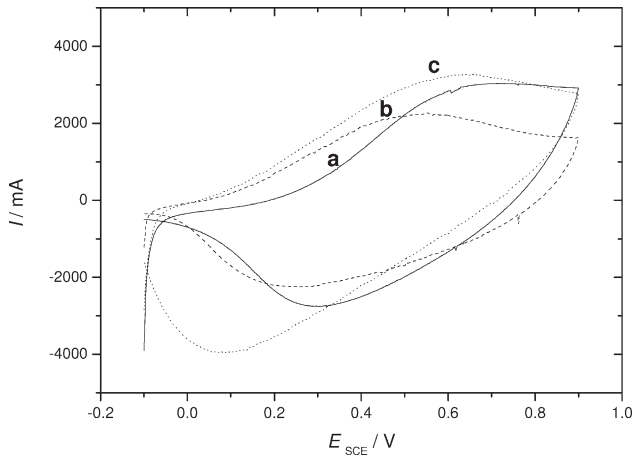

Figure 3. CVs of a gold electrode for (a) PNMPy (solid line), (B) PNMPy-TiO_2 (dashed line), and (C) PNMPy-ZnO (dotted line) nanocomposite polymer films in a blank solution containing ACN +0.1*M* $LiClO_4$ nonaqueous solution in the potential range of $-0.10 < E_{SCE} < 0.90$ V at $dE/dt = 50$ mV s^{-1}, respectively.

to yield a practical means of donating a wide range of conductivities and various patterns of charging–discharging properties of cathode active material of lithium secondary batteries.[14]

EXPERIMENTAL

Reagents and Solvent

N-Methylpyrrole (NMPy) (Aldrich, 99%) was used after purification. Li and $LiClO_4$ (Aldrich Chemie, 99%) used as electrolyte were dried under vacuum. Acetonitrile (ACN) (Merck), water content as determined by Karl Fischer method < 0.05%) was used as received and kept over molecular sieve. Titanium (IV) dioxide (TiO_2, mean diameter 30 nm, Degussa Company, Germany) powder with 80% anatase and 20% rutile phases were used. The ZnO nanocrystals with hexagonal quartzite form and average particle size of 25 nm have been prepared by sol–gel method.

Electrosynthesis of PNMPy and Nanocomposites Materials

Monomers and supporting electrolyte concentrations were $[NMPy] = 0.1M$, $[LiClO_4] = 0.1M$, $[TiO_2] = 0.1M$, and $[ZnO] = 0.1M$. After vigorous mixing and nitrogen purging (10 min), electropolymerization was affected by scanning the electrode potential accompanied with stirring between

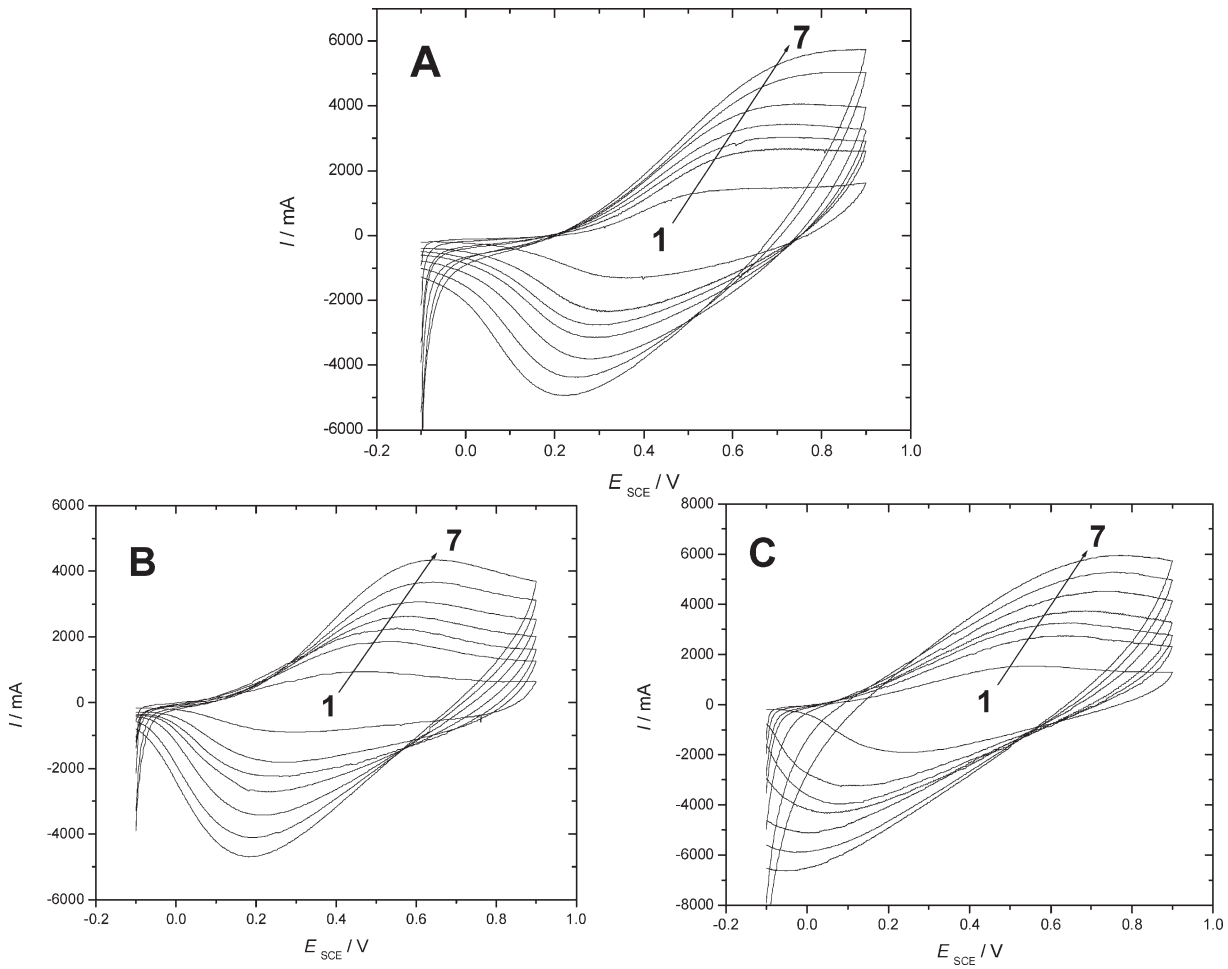

Figure 4. Scan rate dependencies of CVs in ACN +0.1*M* $LiClO_4$ nonaqueous solution for (A) PNMPy, (B) PNMPy-TiO_2, and (C) PNMPy-ZnO nanocomposite polymer films in the potential range of $-0.10 < E_{SCE} < 0.90$ V. $dE/dt = 20$ (1), 40 (2), 50 (3), 60 (4), 80 (5), 100 (6), and 120 (7) mV s^{-1}, respectively.

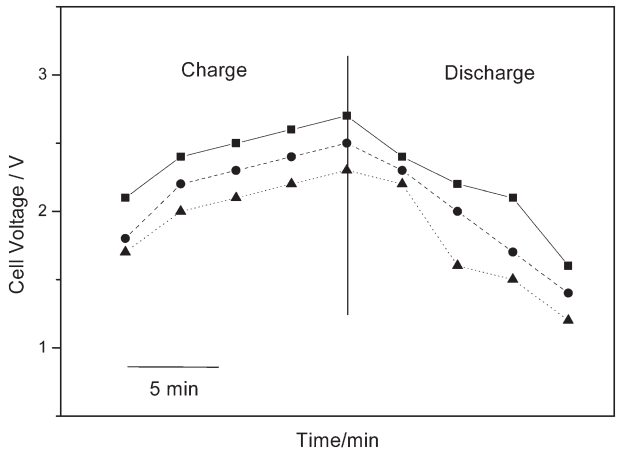

Figure 5. Charging–discharging curves for Li/$LiClO_4$/PNMPy (solid line), Li/LiClO4/PNMPy-TiO_2 (dashed line), and Li/$LiClO_4$/PNMPy-ZnO (dot line) batteries at a constant current of 0.1 mA cm^{-2} in 0.1*M* $LiClO_4$/ACN. Films were polymerized with 1.5 C cm^{-2}.

$-0.10 < E_{SCE} < 0.90$ V for samples at a scan rate of 50 mV s^{-1}. The electropolymerization of nanocomposites under magnetic stirring leads to the formation of thicker and homogenous polymer nanocomposite films on gold electrode containing a significant quantity by weight. Stirring (120 cycle per minute) will keeps the nano-oxide materials in suspension and causes the nanoparticles to be continuously in contact with the electrode surface where the composite films are being deposited. As the cycling continues, a steady-state voltammograms are reached after several scans.

Characterization and Measurement Methods

Cyclic voltammetry were performed using a Behpajoh model BHP/2062 an Autolab model PGSTAT 20 potentiostat/galvanostat. For cyclic voltammetry (CV), a three compartment cell and three electrode, the saturated calomel electrode (SCE) was used as reference electrode, the working and auxiliary electrodes were gold sheets of ~0.4 and 1.0 cm^2 (from AZAR electrode), respectively. A Li/$LiClO_4$/polymer battery was assembled with a polymer cathode and a Li anode pressed onto a Ni expanded mesh. The cell was placed in a small container purged with nitrogen gas tightly sealed. For *in situ* UV–visible spectroscopy, an ITO coated glass sheet (Praezisions Glas & Optik, Germany, $R = 20 \pm 5$ ohm cm^{-2}) was used as a working electrode. UV–visible spectra were recorded with the polymer nanocomposite films deposited on an optically transparent ITO-glass electrode in the supporting electrolyte solution (ACN + 0.1*M* $LiClO_4$) in a standard 10-mm cuvette using a UV–visible spectrophotometer Perkin Elmer, 55 OSD. A cuvette with the same solution and an uncoated ITO glass was placed in the reference beam. Spectra were recorded at increasingly positive electrode potentials; in a few cases, spectra were recorded in the negative-going potential direction in order to test reversibility. The sample morphology have been studied using TEM (Philips XL) and a SEM (Hitachi model S-4160 microscope) accompanied with a sputter coater BAL-TEC, model SCD050. Scanning electron microscope with secondary electron detector (SE) is used to observe the surface of detector precisely. For *in situ* resistivity measurements, a band-gap gold electrode (electrodes made by AZAR electrode) was used as working electrodes.[36] The instrument for conductivity measurement was made by Sama Research Center. The two strips of the band-gap electrode are spaced apart only around 0.08–0.10 mm; this gap can easily be bridged by deposition of conducting polymers. The length of the gap is 3–4 mm. The polymer films are deposited electrochemically on the electrode strips as desired, even very thin films usually form good bridges over the gap between the electrodes. Before each polymer deposition, the electrode was polished with fine emery paper (1000 grit) and alumina (1 μm) to remove the previously deposited material, washed with water, and cleaned ultrasonically.[37] Infrared spectra were recorded on a Perkin Elmer FT-IRGX spectrometer using the KBr pellet technique. All experiments were performed at room temperature with nitrogen-purged solutions.

RESULTS AND DISCUSSIONS

Cyclic Voltammetry and Charge–Discharging Behavior of PNMPy, PNMPy-TiO_2, and PNMPy-ZnO

Figure 1 shows the initial CVs for 0.1*M* NMPy, 0.1*M* NMPy-TiO_2, and 0.1*M* NMPy-ZnO in ACN + 0.1*M* $LiClO_4$ nonaqueous solution in the potential range of $-0.10 < E_{SCE} < 0.90$ V at $dE/dt = 50$ mV s^{-1} on a gold electrode. In the positive going scan, there is a steep current increase at about $E_{SCE} = 0.67$, 0.69, and 0.71 V for NMPy, NMPy-TiO_2, and NMPy-ZnO, respectively. In the negative going scan trace crossing occurs at about $E_{SCE} = 0.66$, 0.70 V, and 0.73 V for NMPy, NMPy-TiO_2, and NMPy-ZnO, respectively. The first step in the formation of the samples is a nucleation process followed by growth of nuclei to continuous films.[38,39] Moreover, this step has been assigned to a comproportionation reaction between oligomeric species and starting monomer molecules at the solution/metal interface.[40,41]

Figure 2 shows the cyclic voltammetry recorded for samples at the range of $-0.10 < E_{SCE} < 0.90$ V at $dE/dt = 50$ mV s^{-1} in ACN + 0.1*M* $LiClO_4$ nonaqueous solution on a gold electrode. During the electropolymerization process, polymers grow on the electrode surface and after the continuous potential scanning, a steady-state voltammograms are reached after 40 scans. For PNMPy, PNMPy-TiO_2, and PNMPy-ZnO [Figure 2(A–C)] during anodic scans, a peaks at around $E_{SCE} = 0.60$, 0.50, and 0.53 V are observed, respectively. During cathodic and reverse scans, peak potentials are located at around $E_{SCE} = 0.16$, 0.19, and 0.23 V for PNMPy, PNMPy-TiO_2, and PNMPy-ZnO, respectively. These peaks correspond to different redox states of PNMPy and PNMPy in the presence of nanoparticles. During the electropolymerization of PNMPy, the potential of the redox couple shifts slightly to more negative values for polymer nanocomposites. The differences between anodic and cathodic peak ($\Delta E_p = E_{pa} - E_{pc}$) of the redox couples for PNMPy, PNMPy-TiO_2, and PNMPy-ZnO are $\Delta E_1 = 0.44$ V, $\Delta E_2 = 0.31$, and $\Delta E_3 = 0.30$ V, respectively. ΔE_p for the PNMPy-TiO_2 and PNMPy-ZnO curves is lower than of PNMPy at which each film begins to grow. The decreases in difference between the anodic and the cathodic peak potentials are indicating better reversibility.

In order to survey the electrochemical response of PNMPy and polymer nanocomposite films, cyclic voltammetry in monomer

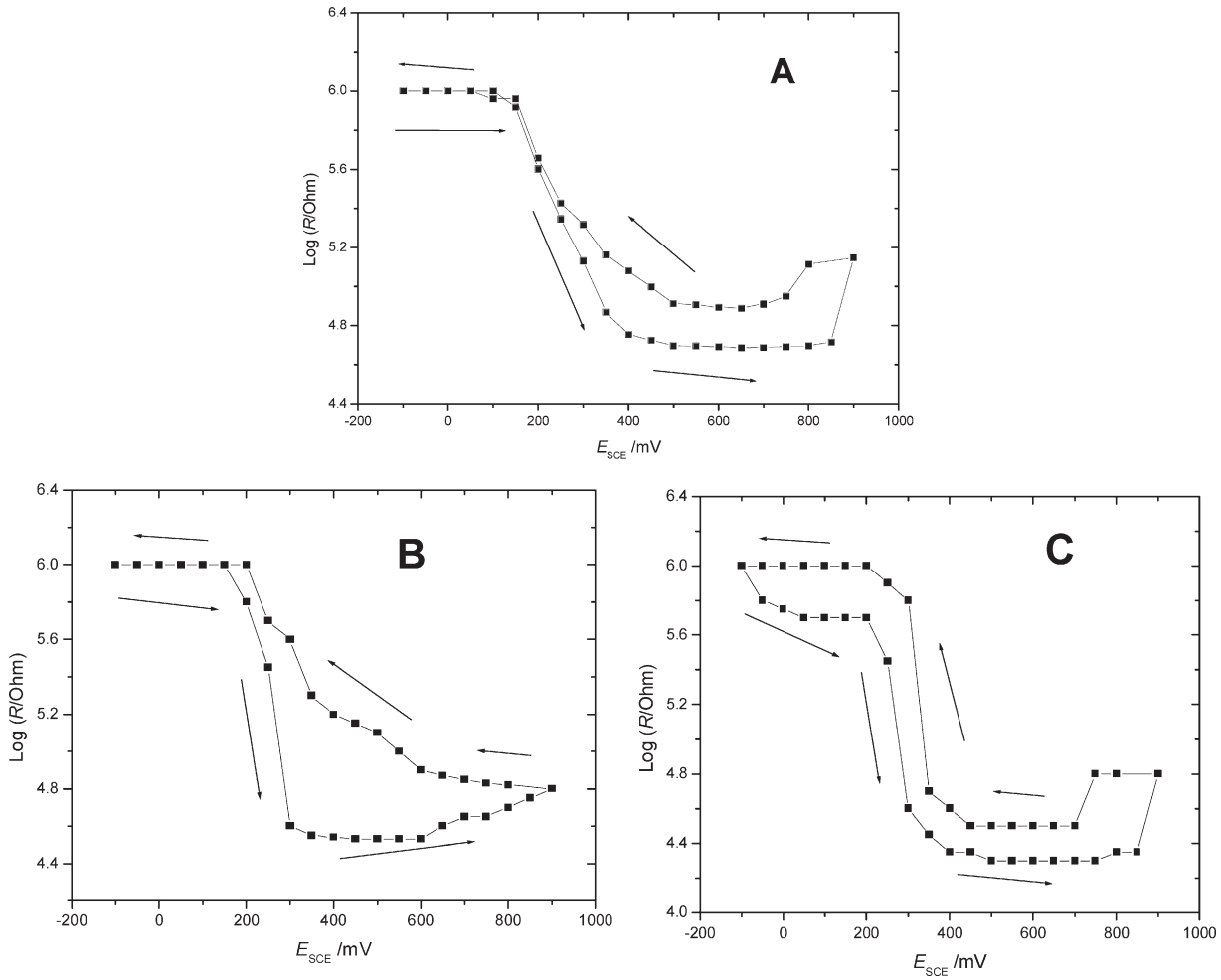

Figure 6. Resistivity vs. electrode potential data for (A) PNMPy, (B) PNMPy-TiO_2, and (C) PNMPy-ZnO nanocomposite polymer films. Films were prepared potentiodynamically by cycling the potential in the potential range of $-0.10 < E_{SCE} < 0.90$ V in ACN + 0.1*M* $LiClO_4$ nonaqueous solution on double band gold electrode at $dE/dt = 50$ mV s^{-1}, respectively.

free background electrolyte solutions at the range of $-0.10 < E_{SCE} < 0.90$ V was employed. The CVs of samples at $dE/dt = 50$ mV s^{-1} and different scan rates ($dE/dt = 20$, 40, 60, 80, 100, and 120 mV s^{-1}) on gold electrode are shown in Figures 3 and 4, respectively. The CVs for all samples seem to be of the same nature, apparently. Nevertheless, differences can be observed especially in the position of the oxidation and reduction peaks. During anodic scans at $dE/dt = 50$ mV s^{-1}(Figure 3), the voltammograms of PNMPy, PNMPy-TiO_2, and PNMPy-ZnO show the oxidation peak potentials located at around $E_{SCE} = 0.70$, 0.51, and 0.60 V, respectively. The reduction potential peak values for PNMPy, PNMPy-TiO_2, and PNMPy-ZnO are located at $E_{SCE} = 0.29$, 0.21, and 0.07 V, respectively.

The anodic and cathodic current peaks for PNMPy-TiO_2 nanocomposite film are located just between those for PNMPy and PNMPy-ZnO films. The results may suggest that a Li/$LiClO_4$/PNMPy-TiO_2 battery possesses intermediate charging and discharging voltages between those of a Li battery assembled with PNMPy and PNMPy-ZnO films. In the case of samples in different scan rates [Figure 4(A–C)] and with increasing the $dE/dt = 20$–120 mV s^{-1}, the redox peaks of polymer nanocomposite shifts to negative values in comparing with PNMPy. With increasing the scan rates, the displacement of the potential peaks is accompanied by increases in the current of the redox peaks from PNMPy to conducting polymer nanocomposites. This is due to the presence of nano metal oxides on PNMPy backbone. In addition, the different potential of redox peaks and CVs of the polymer nanocomposites compared to PNMPy in blank solution inhibits the effect of nanoparticle materials on polymer chains.

Charge–discharging curves of Li/$LiClO_4$/PNMPy, Li/$LiClO_4$/PNMPy-TiO_2, and Li/$LiClO_4$/PNMPy-ZnO batteries at a constant current of 0.1 mA cm^{-2} in 0.1*M* $LiClO_4$/ACN with 1.5 C cm^{-2} formation charges are displayed in Figure 5. The Li/$LiClO_4$/PNMPy-TiO_2 battery gives intermediate curves between other batteries. The discharging behavior of the Li/$LiClO_4$/PNMPy-TiO_2 battery became flatter than other batteries indicating slightly better discharging characteristics. The charging–discharging behavior for Li/$LiClO_4$/PNMPy and Li/$LiClO_4$/PNMPy-ZnO may depend on their film thickness. However, it

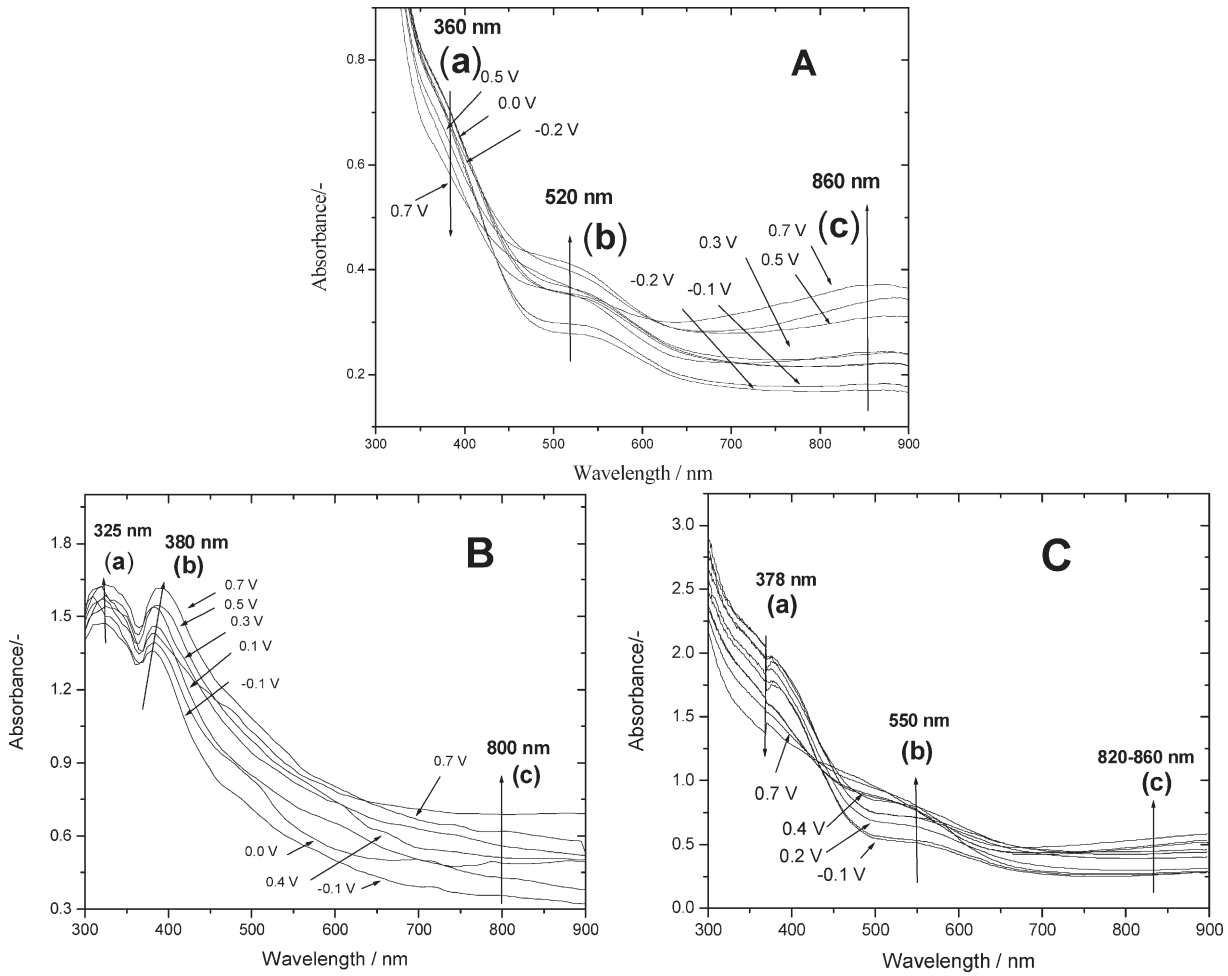

Figure 7. *In situ* UV–visible spectra for (A) PNMPy, (B) PNMPy-TiO_2, and (C) PNMPy-ZnO nanocomposite polymer films deposited potentiodynamically on ITO electrode in the potential range of $-0.10 < E_{SCE} < 0.90$ V in ACN $+0.1M$ $LiClO_4$ nonaqueous solution at different electrode potentials, respectively.

is supposed that the polymer and polymer nanocomposite films have almost the same thickness.

In Situ Resistivity Measurements of PNMPy, PNMPy-TiO_2 and PNMPy-ZnO

Figure 6 shows the resistivity versus the applied electrode potential plots of PNMPy and polymer nanocomposite films in ACN + $0.1M$ $LiClO_4$ nonaqueous solution. For *in situ* resistivity measurements, PNMPy, PNMPy-TiO_2, and PNMPy-ZnO were deposited potentiodynamically by cycling the potentials from $-0.10 < E_{SCE} < 0.90$ V in supporting electrolyte solution at 50 mV s^{-1} on a gold band gap electrode, respectively. A problem associated with the *in situ* resistivity technique is the deposition of different polymer films of identical thickness across the insulating gap. As mentioned elsewhere,[36] this inherent problem can be solved approximately by adjusting experimental conditions (e.g., number of electrode potential cycles or time of electrolysis during deposition) to values resulting in comparable films with similar redox capacities. Moreover, if it can be determined, film thickness as deduced from, for example CV of the deposited polymer films recorded before each series of conductivity measurements in the monomer free electrolyte solution. The plot for PNMPy [Figure 6(A)] shows a single sharp resistivity decrease by 1.3 orders of magnitude at $E_{SCE} = 0.20$, at higher potentials it remains almost constant up to $E_{SCE} = 0.80$ V and then increases again up to $E_{SCE} = 0.90$ V. Minimum resistivity can be observed in the range of $0.40 < E_{SCE} < 0.80$ V. Like PNMPy, the plots for PNMPy-TiO_2 and PNMPy-ZnO nanocomposite films [Figure 6(B,C)] show a single resistivity change by 1.55 and 1.40 order of magnitudes at $E_{SCE} = 0.15$ and 0.20 V, respectively. The resistivity for PNMPy-TiO_2 remains almost constant up to $E_{SCE} = 0.60$ V and then increase up to $E_{SCE} = 0.90$ V by 0.3 order of magnitude. Minimum resistivity can be observed in the range of $0.35 < E_{SCE} < 0.60$ V. For PNMPy-ZnO nanocomposite films, the resistivity remains almost constant from $E_{SCE} = 0.50$ to 0.75 V and then increase up to $E_{SCE} = 0.90$ V by 0.5 order of magnitude. Minimum resistivity can be observed in the range of $0.50 < E_{SCE} < 0.75$ V.

The resistivity of PNMPy-TiO_2 and PNMPy-ZnO nanocomposite films are lower than that of PNMPy by around 0.20 and 0.30 orders of magnitudes, respectively. These observations demonstrate that by adding the nano metal oxide in NMPy solution feed, the resistivity of the polymer nanocomposites

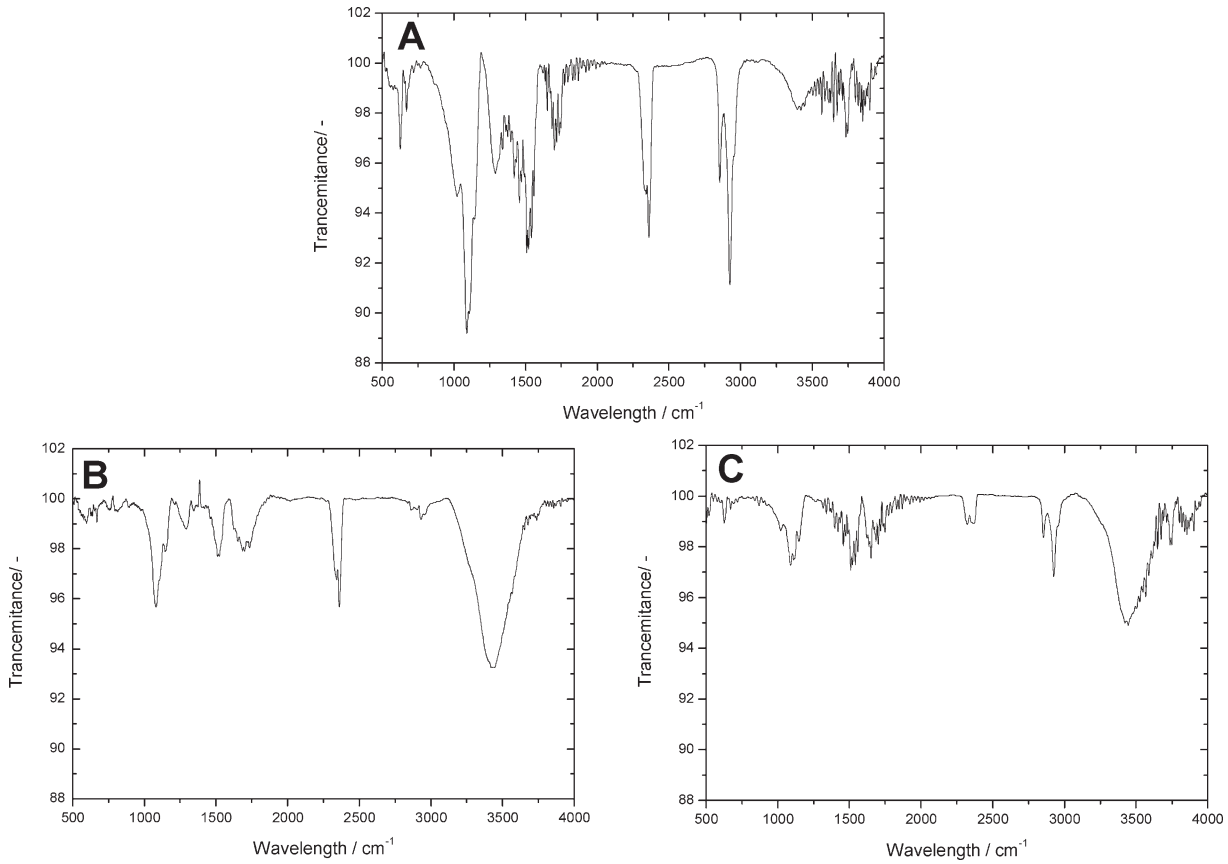

Figure 8. FTIR transition spectra of (A) PNMPy, (B) PNMPy-TiO_2, and (C) PNMPy-ZnO nanocomposite polymer films.

decreases. This may be caused by influence of nano-oxide materials on the growth of PNMPy on surface electrode. It can be seen that the surface resistance value decreases rapidly with the NMPy monomer in the presence of oxide materials. A larger amount of monomer units in the polymer nanocomposite films backbone yield a more extended π-conjugation system along the nanocomposite films. This also implies that nanocomposite films induce an increase in the degree of PNMPy backbone conjugation.

In Situ UV–Visible Spectroscopy of PNMPy, PNMPy-TiO_2, and PNMPy-ZnO

Figure 7 shows the *in situ* UV–visible spectra of PNMPy, PNMPy-TiO_2, and PNMPy-ZnO prepared potentiodynamically by cycling the potentials between $-0.10 < E_{SCE} < 0.90$ V in ACN + 0.1*M* $LiClO_4$ nonaqueous solution on ITO electrodes. The observed spectral features are attributed to three transitions (labeled: (a), (b), and (c)) between the electronic levels, including valence band, conduction band, and polaron or bi-polaron bands, respectively (For a detailed discussion see e.g. Ref. 42). During oxidation of the PNMPy film [Figure 7(A)], a decrease in absorbance around 380 nm and an increase in the band between 520 nm and 860 nm were observed.[43] Moreover, with increasing the applied potential from $E_{SCE} = -0.10$–0.70 V, the absorbance between 480 nm to 550 nm increased.[43,44] The first transition (a) is assigned to the $\pi \rightarrow \pi^*$ transition of the neutral PNMPy film, there is only one allowed optical transition. In the polaron state, there are two transitions labeled (b) and (c), around 540 nm and 800 nm, corresponding to a transition from the valence band to the antibinding polaron state and a transition from the binding to the antibinding polaron state.[43] Transition (b) may also be caused by an excitation from the valence band into the bi-polaron state with maximum absorbance at $E_{SCE} = 0.50$–0.70 V.[37,43,45] At low doping levels, an increase in the absorbance is attributed to the polarons appearing before bi-polaron spectra. The changes in absorbance of the PNMPy coated electrode are accompanies by visible reversible changes of film color, ranging from violet at $E_{SCE} = 0.00$ V to black at $E_{SCE} = 0.70$ V, representing the electrochromic properties of the PNMPy films clearly.

The *in situ* spectra for nanocomposite polymers are different from PNMPy films clearly. The UV–visible absorption spectra of PNMPy-TiO_2 films [Figure 7(B)] recorded at different applied electrode potentials between $-0.10 < E_{SCE} < 0.70$ V shows three absorption bands at 325, 380, and 800 nm. The bands labeled (a) in Figure 7(B) is assigned to an absorption around 325 nm which is attributed to the $\pi \rightarrow \pi^*$ transition of the NMPy-TiO_2 moiety. The bands labeled (c) refers to a broad absorption with a maximum around 700–900 nm in the fully oxidized black form of PNMPy-TiO_2. Between these limits the film color is violet-white due to a third absorption labeled (b) that develops at 400–600 nm with maximum absorbance at $E_{SCE} = 0.70$ V. This absorption is assigned to the high-energy polaron transition.[46,47] In the case of

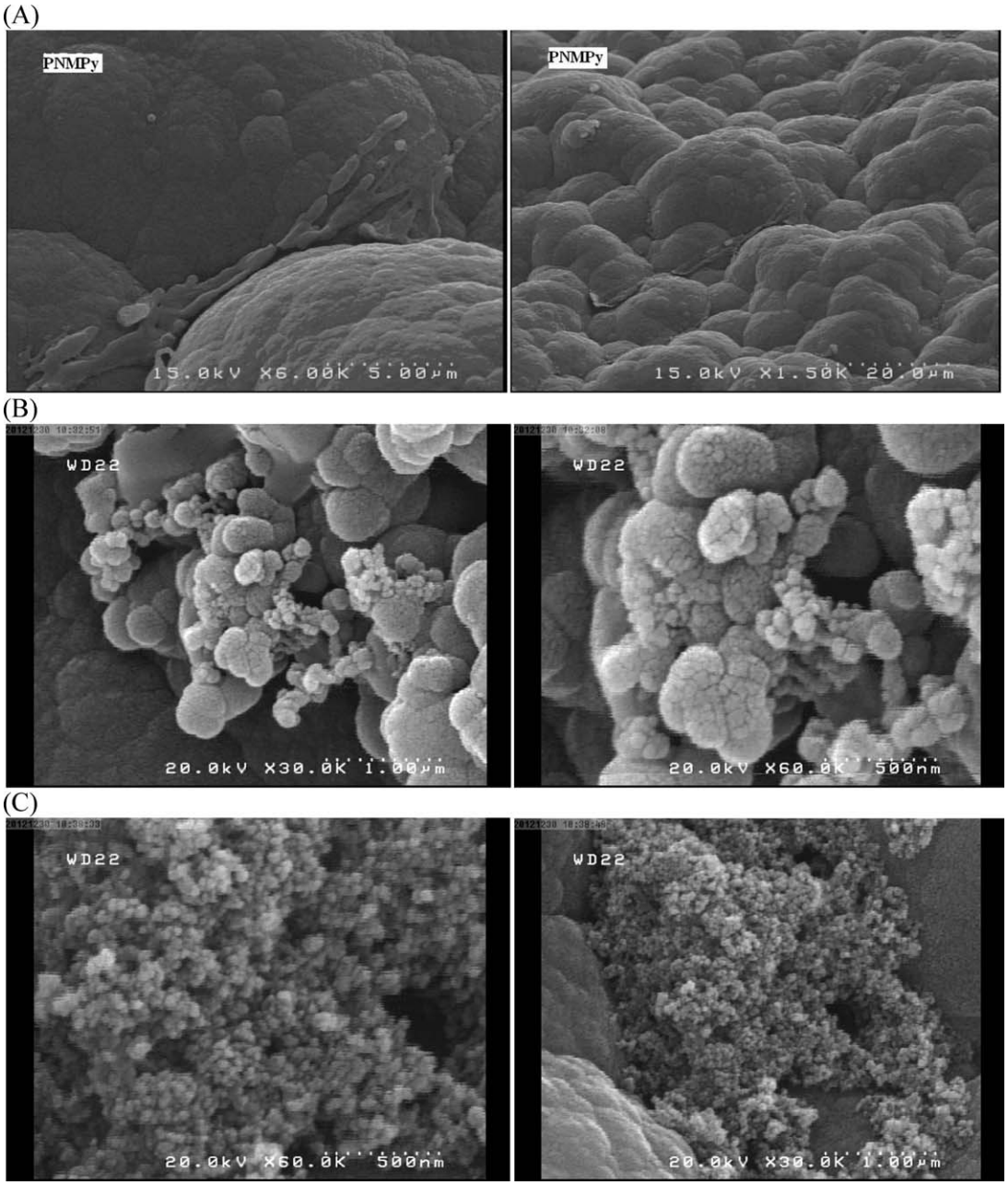

Figure 9. SEM micrographs of (A) PNMPy, (B) PNMPy-TiO_2, and (C) PNMPy-ZnO nanocomposite polymer films.

PNMPy-ZnO during oxidation of the polymer film, a decrease in absorbance around 378 nm and an increase in the band between 550 nm and 820–860 nm were observed.[43] With increasing the applied potential from $E_{SCE} = -0.10$ to 0.70 V, the absorbance between 480 to 560 nm increased [see Figure 4(C)]. The spectra features may indicate the effect of nano metal oxides in polymer backbones. It can be seen that for nanocomposite films, there are some shifts in the peaks compared to the PNMPy films. It may be related to the influence of nano metal particles on the doping of conducting PNMPy or coordinate complex formation between nano metal oxide particles and NMPy monomer before *in situ* electro-polymerization. Moreover, the intensities of the spectrum as compared to the PNMPy film were changed due to the absorption property of nano metal particles. The influence of addition of TiO_2 and ZnO on the optical behavior of PNMPy is caused by the absorption and change of wavelengths (see Figure 7). In addition, the absorbance spectrum confirmed the presence of TiO_2 and ZnO in PNMPy nanocomposite matrix at the different wavelengths.[21]

FTIR Spectroscopy Studies of PNMPy, PNMPy-TiO_2, and PNMPy-ZnO

FTIR spectroscopic measurements were carried out to investigate the structures of PNMPy, PNMPy-TiO_2, and PNMPy-

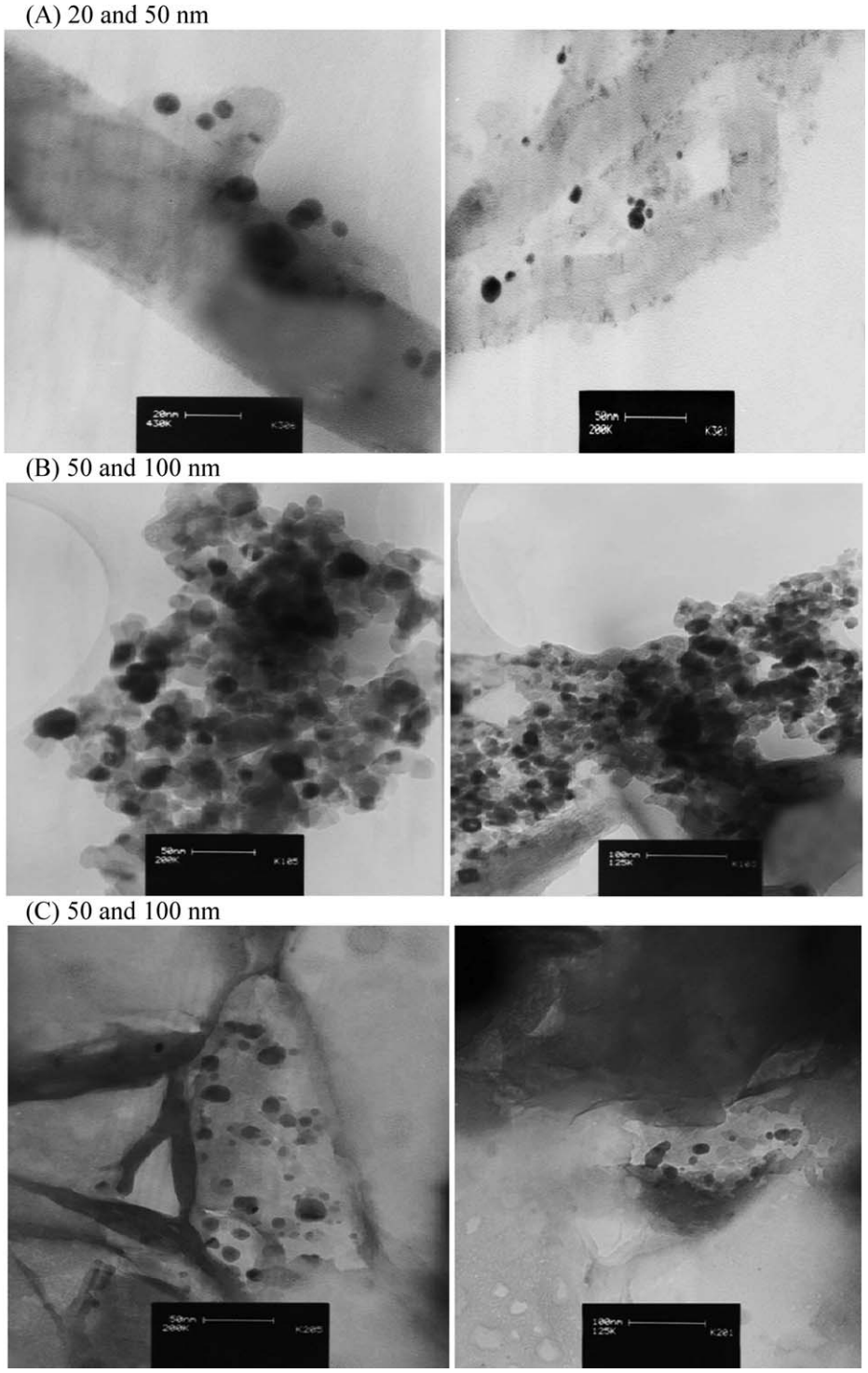

Figure 10. TEM micrographs of (A) PNMPy, (B) PNMPy-TiO_2, and (C) PNMPy-ZnO nanocomposite polymer films.

ZnO nanocomposite films. Figure 8 shows the FTIR spectra of PNMPy, PNMPy-TiO_2, and PNMPy-ZnO nanocomposite polymers in the range of 500–4000 cm^{-1}. The IR spectra of PNMPy films [Figure 8(A)] have been already discussed by us and other researchers and it has been observed that the spectra of the films prepared in different laboratory conditions do not coincide, due to the different extents of delocalization of charge and their prominent vibrational modes in the roughly finger print region at the same position.[48–50] The characteristic vibrational bands associated with PNMPy are present in PNMPy-TiO_2 [Figure 8(B)] and PNMPy-ZnO [Figure 8(C)] with a considerable shift, which indicates the synthesis of

nanocomposite polymer films. The principal vibrational bands observed here for C—H stretching vibrations of the *N*-substituted methyl group is present in PNMPy at 2927 cm^{-1} and with a weaker intensity in PNMPy-TiO_2 and PNMPy-ZnO at around 2932 and 2930 cm^{-1}, respectively. The band due to C=C stretching observed in PNMPy at 1522 cm^{-1} is shifted to 1532 and 1518 cm^{-1} in PNMPy-TiO_2 and PNMPy-ZnO nanocomposite polymer films. The band at 1288 cm^{-1} corresponding to the C—N in-plane bending modes in PNMPy is shifted to 1294 cm^{-1} in PNMPy-TiO_2. However, it is absent in the spectrum of PNMPy-ZnO. The band due to C=C stretching observed in PNMPy at 1522 cm^{-1} is shifted to 1532 and 1518 cm^{-1} in PNMPy-TiO_2 and PNMPy-ZnO polymer nanocomposite films, respectively. The band at 1459 cm^{-1} corresponding to the stretching and bending mode of aromatic alkenes in PNMPy shifted to the very week band at 1452 cm^{-1} in polymer nanocomposite films. The sharp band due to C=N stretching or C=H in plane deformation observed in PNMPy at 1092 cm^{-1} is shifted to 1080 and 1103 cm^{-1} in PNMPy-TiO_2 and PNMPy-ZnO nanocomposite polymer films. The intensity of those bands for nanocomposite polymer films is decreased. Moreover, the intensity of broad band at around 3422 cm^{-1} due to C—H stretching is shifted and increased for PNMPy-TiO_2 and PNMPy-ZnO. The interactions between some metal oxide particles and conducting polymers was reported previously.[31,51] The shifts of wavelengths and intensity changing of the vibrational peaks in nanocomposite films as compared to the PNMPy may be ascribed to the formation of hydrogen bonding between TiO_2 and ZnO with C—H group of PNMPy molecular chains on the surface of nano metal oxide particles.

The Morphological Studies of PNMPy, PNMPy-TiO_2, and PNMPy-ZnO

The morphology of PNMPy, PNMPy-TiO_2, and PNMPy-ZnO nanocomposite polymers was characterized by SEM and TEM analyses (Figures 9 and 10). The SEM of PNMPy reveals a smooth surface with isolated nodules and large particle aggregations with a cauliflower form growing over it [Figure 9(A)].[52] The morphologies of the PNMPy-TiO_2 and PNMPy-ZnO nanocomposite polymers are very similar to those of PNMPy and show the nanoparticles in the presence of the PNMPy. The SEM micrograph of nanocomposite polymers suggests that the structures of PNMPy were nano-oxide particles [see Figure 9(B,C)]. Thus, the nano-oxide particles can modify the morphology and properties of the PNMPy films.

The TEM of PNMPy, PNMPy-TiO_2, and PNMPy-ZnO nanocomposite polymers were studied to better understand the role of nanoparticle in the PNMPy films. The TEM images of TiO_2 and ZnO nanoparticles (which used here) with a particle size about 30 nm were reported previously.[52–54] The TEM micrograph of nanocomposite polymer films [Figure 10(B,C)] suggests that the inorganic semiconductor particles were incorporated in organic conducting PNMPy, which consequently modify the morphology of the PNMPy films significantly. More detail discussion for SEM or TEM is not accessible.

CONCLUSIONS

PNMPy, PNMPy-TiO_2, and PNMPy-ZnO nanocomposite polymer films were synthesized electrochemically by cycling the potential on gold electrode in ACN. The PNMPy and nanocomposite polymers were characterized by CV, charging–discharging measurements, *in situ* conductivity measurements, *in situ* UV–visible, FTIR spectroscopy, SEM, and TEM analyses. The results of charging and discharging behavior suggest that a Li/$LiClO_4$/PNMPy-TiO_2 battery possesses intermediate voltages between those of a Li battery assembled with PNMPy and PNMPy-ZnO films. The nanocomposite polymer films show pronounced electrochemical activity. *In situ* conductivity measurements of the obtained PNMPy film were found to be lower than PNMPy-TiO_2 and PNMPy-ZnO nanocomposite polymer films. The results of FTIR show that the characteristic vibration bands associated with PNMPy are present in polymer nanocomposites with a considerable shift and different intensity indicating formation of true polymer hybrid materials. The SEM analysis of nanocomposite polymer films shows the nanoparticles in polymer backbone. The TEM images suggest that the nano oxide particles were incorporated in conducting PNMPy, which consequently modifies the morphology of the polymer significantly. In addition, the results indicate the effect of nano-oxide materials on the electro-polymerization process and polymer backbones.

ACKNOWLEDGMENTS

This work was sponsored by Bu-Ali Sina University and authors thank Miss. Eng. F. Hosseini (Sama Research Center) for her help in making required instruments for measuring the *in situ* resistivity and also thank AZAR electrode for preparing all electrodes. They also thank to Prof. Dr. S. Azizian for generous donations of ZnO and TiO_2 nanoparticles.

REFERENCES

1. Nadagouda, M. N.; Varma, R. S. *Macromol. Rapid Commun.* **2007**, *28*, 2106.
2. Skotheim, T. A.; Elsenbauer, R. L.; Reynolds, J. R., Eds. Handbook of Conducting Polymers; Marcel Dekker: New York, **1998**.
3. Karim, M. R.; Yeum, J. H.; Lee, M. Y.; Lee, M. S.; Lim, K. T. *Polym. Adv. Technol.* **2008**, *20*, 639.
4. Mahmoud, W. E.; Chang, Y. C.; Al-Ghamdi, A. A.; Al-Marzouki, F.; Bronstein, L. M. *Polym. Compos.* **2013**, *34*, 299.
5. Arjomandi, J.; Kakaei, Z. *J. Electrochem. Soc.* **2014**, *161*, 53.
6. Wang, L. X.; Li, X. G.; Yang, Y. L. *React. Funct. Polym.* **2001**, *47*, 125.
7. Ryu, K.; Park, N.; Kim, K.; Lee, Y.; Park, Y.; Lee, S.; Jeong, C.; Joo, J.; Chang, S. *Synth. Met.* **2003**, *135*, 397.
8. Holze, R.; Nalwa, H. S., Eds. Handbook of Advanced Electronic and Photonic Materials and Devices; Academic: San Diego, CA, **2001**; Vol. *8*, p 209.
9. Genies, E. M.; Syed, A. A. *Synth. Met.* **1985**, *21*, 10.

10. Rohde, N.; Eh, M.; Geissler, U.; Hallensleben, M. L.; Voigt, B.; Voigt, M. *Adv. Mater.* **1995**, *7*, 401.
11. Benincori, T.; Brenna, E.; Sannicoló, F.; Zotti, G.; Zecchin, S.; Schiavon, G.; Gatti, C.; Frigerio, G. *Chem. Mater.* **2000**, *12*, 1480.
12. De la Blanca, E. S.; Redondo, M. I.; Garcìa, M. V.; Raso, M. A.; Tortajada, J.; Gonz'alez-Tejera, M. J. *Synth. Met.* **2003**, *139*, 145.
13. Skotheim, T. A.; Elsenbaumer, R. L.; Reynolds, J. R., Eds. Handbook of Conducting Polymers; Marcel Dekker: New York, 1986.
14. Naoi, K.; Hirabayashi, T.; Tsubota, I.; Osaka, T. *Bull. Chem. Soc. Jpn.* **1987**, *60*, 363.
15. Zhang, L.; Zhang, C.; Lian, J. *Biosens. Bioelectron.* **2008**, *24*, 690.
16. Dhand, C.; Arya, S. K.; Pal Singh, S.; Singh, B. P.; Datta, M.; Malhotra, B. D. *Carbon* **2008**, *46*, 1727.
17. He, B. L.; Dong, B.; Wang, W.; Li, H. L. *Mater. Chem. Phys.* **2009**, *114*, 371.
18. Kaneto, K.; Asano, T.; Takashima, W. *Jpn J. Appl. Phys.* **1991**, *30*, 215.
19. Yuen, J. D.; Dhoot, A. S.; Namdas, E. B.; Coates, N. E.; Heeney, M.; McCulloch, I.; Moses, D.; Heeger, A. J. *J. Am. Chem. Soc.* **2007**, *129*, 14367.
20. Kaneto, K.; Asano, T.; Takashima, W. *Jpn. J. Appl. Phys.* **1991**, *30*, 365.
21. Arjomandi, J.; Tadayyonfar, S. *Polym. Compos.* **2014**, *35*, 351.
22. Gustafsson, G.; Cao, Y.; Treacy, G. M.; Klavetter, F.; Colaneri, N.; Heeger, A. *Nature* **1992**, *357*, 477.
23. Sailor, M. J.; Ginsburg, E. J.; Gorman, C. B.; Kumar, A.; Grubbs, R. H.; Lewis, N. S. *Science* **1990**, *249*, 1146.
24. Yavuz, A. G.; Gök, A. *Synth. Met.* **2007**, *157*, 235.
25. Zhang, J.; Feng, H.; Hao, W.; Wang, T. *Ceram. Int.* **2007**, *33*, 785.
26. Alam, J.; Riaz, U.; Ahmad, S. *J. Magn. Magn. Mater.* **2007**, *314*, 93.
27. Song, G.; Han, J.; Guo, R. *Synth. Met.* **2007**, *157*, 170.
28. Yu, C.; Zhai, J.; Li, Z.; Wan, M.; Gao, M.; Jiang, L. *Thin Solid Films* **2008**, *516*, 5107.
29. Li, J.; Zhu, L.; Wu, Y.; Harima, Y.; Zhang, A.; Tang, H. *Polymers* **2006**, *47*, 7361.
30. Mahmoud, W. E. *J. Phys. D. Appl. Phys.* **2009**, *42*, 155502.
31. He, Y. *Appl. Surf. Sci.* **2005**, *249*, 1.
32. Zheng, J.; Li, G.; Ma, X.; Wang, Y.; Wu, G.; Cheng, Y. *Sens. Actuators B.* **2008**, *133*, 37.
33. Zhang, L. X.; Liu, P.; Su, Z. X. *Polym. Degrad. Stab.* **2006**, *91*, 2213.
34. Ram, M. K.; Yavuz, O.; Lahsangah, V.; Aldissi, M. *Sens. Actuators B.* **2005**, *106*, 750.
35. Mahmoudian, M. R.; Basirum, W. J.; Alias, Y. *Appl. Surf. Sci.* **2011**, *257*, 3702.
36. Holze, R.; Lippe, J. *Synth. Met.* **1990**, *38*, 99.
37. Arjomandi, J.; Holze, R. *J. Solid State Electrochem.* **2013**, *17*, 1881.
38. Asavapiriyanont, S.; Chandler, G.; Gunawardena, G.; Pletcher, D. *J. Electroanal. Chem.* **1984**, *177*, 245.
39. Asavapiriyanont, S.; Chandler, G.; Gunawardena, G.; Pletcher, D. *J. Electroanal. Chem.* **1984**, *177*, 229.
40. Heinze, J.; Frontana-Uribe, B. A.; Ludwigs, S. *Chem. Rev.* **2010**, *110*, 4724.
41. Heinze, J.; Rasche, A.; Pagels, M.; Geschke, B. *J. Phys. Chem. B* **2007**, *111*, 989.
42. Arjomandi, J.; Holze, R. *Centr. Europ. J. Chem.* **2008**, *6*, 199.
43. Arjomandi, J.; Holze, R. *Synth. Met.* **2007**, *157*, 1021.
44. Hyodo, K.; MacDiarmid, A. *Synth. Met.* **1985**, *11*, 167.
45. Yakushi, K.; Lauchlan, L.; Clarke, T.; Street, G. *J. Chem. Phys.* **1983**, *79*, 4774.
46. Bredas, J.; Scott, J.; Yakushi, K.; Treet, G. S. *Phys. Rev. B. Condens Mater.* **1984**, *30*, 1023.
47. Zotti, G.; Schiavon, G. *Synth. Met.* **1989**, *30*, 151.
48. Arjomandi, J.; Safdar,S.; Malmir, M. *J. Electrochem. Soc.* **2012**, *159*, 73.
49. Köleli, F.; Arslan, Y.; Düdükcü, M. *Synth. Met.* **2002**, *129*, 47.
50. Tian, B.; Zerbi, G. *J. Chem. Phys.* **1990**, *92*, 3886.
51. Paul, G. K.; Bhaumik, A.; Patra, A. S.; Bera, S. K. *Mater. Chem. Phys.* **2007**, *106*, 360.
52. Arjomandi, J.; Eshghi, S. *J. Electroanal. Chem.* **2013**, *690*, 36.
53. Jafari, S.; Azizian, S.; Jaleh, B. *Colloids. Surf. A. Physicochem. Eng. Asp.* **2011**, *384*, 618.
54. Jaleh, B.; Ashrafi, G.; Gholami, N.; Azizian, S.; Golbedaghi, R.; Habibi, S.; Parsian, H. *Adv. Mater. Res.* **2011**, *1205*, 403.